Lung mammary metastases but not primary tumors induce accumulation of atypical large platelets and their chemokine expression

Cell Reports

Lung Mammary Metastases but Not Primary Tumors Induce Accumulation of Atypical Large Platelets and Their Chemokine Expression

Graphical Abstract

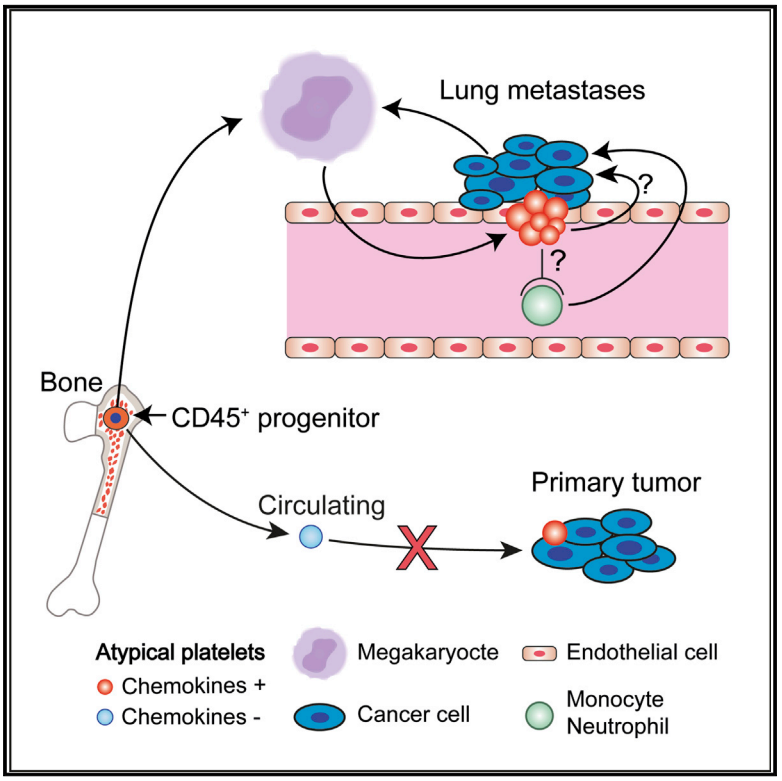

Highlights

- Atypical large platelets are specifically enriched in lung metastases
- They are produced by lung-resident megakaryocytes and highly express chemokines
- They share markers with endothelial cells but have a distinct bone marrow origin

Authors

Wei Zheng, Hui Zhang, Dejian Zhao, Jinghang Zhang, Jeffrey W. Pollard

Correspondence

wei.zheng@mssm.edu (W.Z.), jeffrey.pollard@einstein.yu.edu (J.W.P.)

In Brief

Zheng et al. show a distinct type of large platelets is specifically enriched in lung metastases but not in primary tumors. Identification of this cell type provides insight into the complexity of the metastatic tumor microenvironment. It also helps clarify confusion about the origin of endothelial progenitor cells.

Zheng et al., 2019, Cell Reports *29*, 1747–1755
November 12, 2019
https://doi.org/10.1016/j.celrep.2019.10.016

CellPress

Cell Reports
Report

Lung Mammary Metastases but Not Primary Tumors Induce Accumulation of Atypical Large Platelets and Their Chemokine Expression

Wei Zheng,[1,5,*] Hui Zhang,[1] Dejian Zhao,[2] Jinghang Zhang,[3] and Jeffrey W. Pollard[1,4,6,*]
[1]Department of Developmental and Molecular Biology, Albert Einstein College of Medicine and Montefiore Medical Center, Bronx, NY 10461, USA
[2]Yale Center for Genome Analysis, Yale University, New Haven, CT 06510, USA
[3]Department of Microbiology & Immunology, Albert Einstein College of Medicine and Montefiore Medical Center, Bronx, NY 10461, USA
[4]MRC Centre for Reproductive Health, Queen's Medical Research Institute, The University of Edinburgh, Edinburgh EH16 4TJ, UK
[5]Present address: Division of Hematology and Oncology, Department of Medicine, Icahn School of Medicine at Mount Sinai, New York, NY 10029, USA
[6]Lead Contact
*Correspondence: wei.zheng@mssm.edu (W.Z.), jeffrey.pollard@einstein.yu.edu (J.W.P.)
https://doi.org/10.1016/j.celrep.2019.10.016

SUMMARY

The tumor microenvironment (TME) at the metastatic site consists of multiple components with considerable cellular heterogeneity. To test whether endothelial cells (ECs) associated with lung metastases express a distinct gene expression program that promotes metastatic growth, we isolated *CD31*$^{+}$/*CD45*$^{-}$ cells from lung mammary cancer metastases for RNA sequencing and found CD44 upregulation. Unexpectedly, the *CD44*$^{+}$ subset did not comprise authentic ECs nor were they bone-marrow-derived *CD45*$^{-}$ endothelial progenitor cells. Instead, they were a population of large platelets that are distinct from regular small platelets. These *CD44*$^{+}$ large platelets were enriched in lung metastases but not primary mammary tumors and upregulated myeloid cell-regulating chemokines indicative of potential regulation of metastasis via indirect mechanisms. Identification of this cellular player in the TME of metastasis suggests a role for the recently identified lung-resident megakaryocytes (MKs) and offers an unexplored route to discover novel mechanisms and an opportunity for therapeutic interventions.

INTRODUCTION

Solid tumors are relatively successfully treated if restricted to the primary site, but current therapeutics are inadequate in metastatic diseases that cause the majority of patient deaths (Steeg, 2016). Anti-angiogenic therapies aim at inhibiting generation of new blood vessels that support tumor growth and have shown some effects in primary cancers, but the benefits for metastatic breast cancer are limited (Potente et al., 2011). Blood vessels are more than passive conduits for delivering nutrients to tumors or for cancer cell dissemination. Instead, they can positively regulate neighboring cells by expression of angiocrine factors (EC-derived paracrine-acting factors) (Butler et al., 2010). However, a comprehensive understanding of what angiocrine factors are at the metastatic site and what biological processes they collectively regulate is fundamentally lacking.

CD31 (also known as PECAM1) is a conventional EC marker that is also expressed to varying degrees in platelets and certain leukocyte subtypes (Lertkiatmongkol et al., 2016). It is also expressed by certain progenitor cells in the bone marrow (BM), including endothelial progenitor cells (EPCs), which are believed to be BM-resident non-hematopoietic progenitors for *CD31*$^{+}$ circulating endothelial cells that can be incorporated into the vessel network at the site of angiogenesis (Bertolini et al., 2006; Gao et al., 2008; Patenaude et al., 2010). However, EPCs have remained a controversial concept, as their contribution to vessels in tumors varies from more than 50% to none, and the exact cell of origin of the BM-derived *CD31*$^{+}$ cells in tumors has not been fully established (Medina et al., 2017; Patenaude et al., 2010).

Another important component of the TME is the tumor-infiltrating myeloid cells that promote tumor growth and metastasis (Kitamura et al., 2015a; Powell and Huttenlocher, 2016). Since inflammation can prime the endothelium to attract myeloid cells to the site of infection, and inflammation and cancer are intricately linked (Grivennikov et al., 2010), it is thus plausible that disseminated cancer cells in secondary organs may redirect the inflammatory response to recruit metastasis-promoting myeloid cells indirectly via activation of the endothelium.

Based on these data, we initially hypothesized that breast cancer cells disseminated to the lung actively regulate non-sprouting vessels that in turn provide signals to enhance metastatic growth, either directly via activation of cancer cells or indirectly via recruitment and regulation of myeloid cells. Unexpectedly, while attempting to address this hypothesis, we uncovered a previously unrecognized population of large platelets enriched specifically in lung metastases but not in primary tumors.

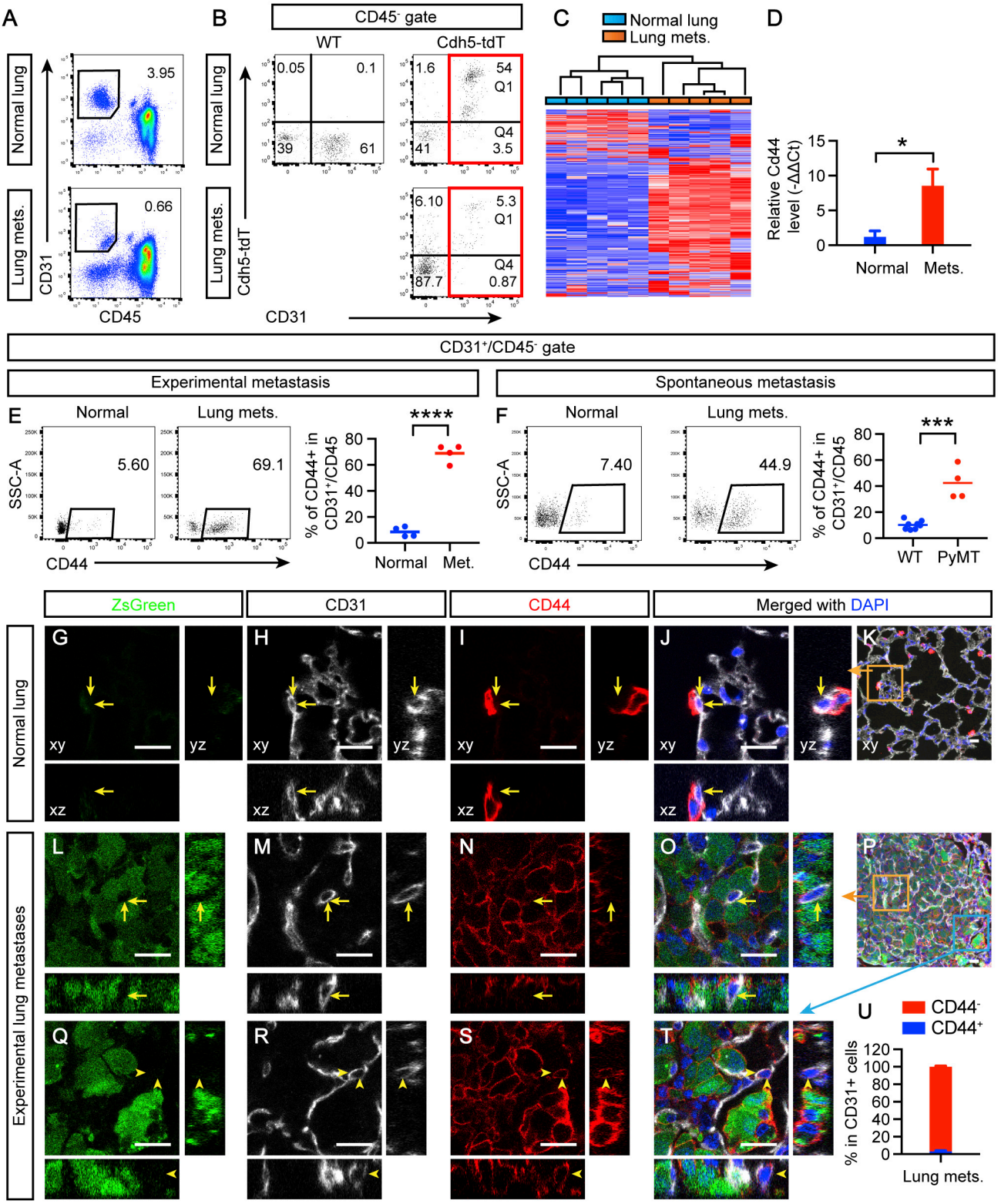

Figure 1. Lung Metastases Induce an Increase of a *CD44*⁺ Subset of *CD31*⁺/*CD45*⁻ Cells that Do Not Appear to Be Endothelial Cells

(A) Lung metastases (mets.) induced by E0771-LG i.v. injection at day 11 were dissected and processed to sort *CD31*⁺/*CD45*⁻ cells and compared with those from the normal lung without tumors.

(legend continued on next page)

RESULTS

Gene Expression Profiling of *CD31*$^+$/*CD45*$^-$ Cells from Lung Metastases Reveals a Distinct *CD44*$^+$ Population

First, we characterized the vessel phenotypes associated with lung metastases using a spontaneous transgene-induced mouse mammary tumor model of breast cancer (MMTV-PyMT, Figures S1A–S1G) (Guy et al., 1992; Lin et al., 2003) and an experimental metastasis model using tail vein injection of a metastatic mammary cancer cell line, E0771-LG (Kitamura et al., 2015b) (Figures S1H–S1N). In both models, no sprouting angiogenesis was observed in metastatic nodules that were visible to naked eyes and were therefore macro-metastases by definition (Figures S1F, S1G, S1I and S1K). Instead, these intratumor vessels maintain their original anatomical structure found in the alveoli of normal lungs (Figures S1F, S1G, and S1J). This contrasts with the sprouting angiogenesis in primary tumors, as evident by dense microvessels with irregular morphology and sprouting filopodia (Figures S1A–S1C). Not until day 13 in the experimental model, when lesions had taken over much of the space of the lung, did sprouting angiogenesis appear (Figures S1L–S1N). These data suggest that sprouting angiogenesis is not required for the initial and intermediate growth into macro-metastases in the lung that is rich in capillary vessels.

To understand whether non-sprouting vessels in the lung promote metastatic growth via angiocrine factors, we isolated ECs from lung metastases at day 11 post-intravenous (i.v.) injection and compared with those of normal lung vessels using RNA sequencing (RNA-seq) (Table S1). The cells were sorted by fluorescence-activated cell sorting (FACS) based on their expression of the EC marker CD31 and negative expression for the pan-leukocyte marker CD45 (Figure 1A). To further confirm the EC identity, we used double-transgenic mice in which the fluorescent protein tdTomato is expressed upon Cre-mediated recombination in cells that express the EC marker *VE-cadherin* (*Cdh5*) (Alva et al., 2006; Madisen et al., 2010). Analysis of lung metastases from these *Cdh5-Cre;Rosa26-loxp-stop-loxp-tdTomato* mice (*Cdh5-tdT* thereafter) showed that most of *CD31*$^+$/*CD45*$^-$ cells were positive for Cdh5-tdT (Figure 1B, Q1/(Q1+Q4) = 86%). Unsupervised hierarchical clustering analysis of the RNA-seq data completely segregated *CD31*$^+$/*CD45*$^-$ cells from normal lungs and dissected lung metastases into two distinct clusters (Figure 1C), indicating a distinct gene expression program in metastases.

To understand how potential factors from this *CD31*$^+$/*CD45*$^-$ population may contribute to metastatic growth indirectly via regulation of myeloid cells, we focused on two of the top ten pathways enriched by the differentially expressed genes related to leukocyte trafficking and function (Table S1, tab "Pathways"). CD44, a transmembrane glycoprotein involved in cell-cell interaction, cell adhesion, and migration (Orian-Rousseau and Ponta, 2015), was identified by the RNA-seq as one of the significantly upregulated genes enriched in these pathways and was also confirmed by qRT-PCR analysis (Table S1, tab "Pathways"; Figure 1D). This upregulation was also confirmed at the protein level by FACS in both experimental and spontaneous models (Figures 1E and 1F).

The *CD44*$^+$ Subset of *CD31*$^+$/*CD45*$^-$ Cells in Lung Metastases Does Not Appear to Be ECs

To analyze the spatial/anatomic information of *CD31*$^+$/*CD45*$^-$ *CD44*$^+$ cells in relation to metastatic tumor cells, we transduced E0771-LG cells with a lentivirus expressing luciferase-ZsGreen (Luc-ZsG) to visualize tumor cells before i.v. injection (Figures 1G, 1L, and 1Q). As expected in the normal lung, ECs forming pulmonary capillaries were *CD44*$^-$ (Figures 1G–1K). Surprisingly, less than 3% *CD31*$^+$ ECs appeared to be *CD44*$^+$ in lung metastases (Figures 1L–1U), in sharp contrast to the 69% observed by flow cytometry (Figure 1E). Similar findings were observed also for the spontaneous metastasis model (Figures 1F and S2). The apparent discrepancy between flow-cytometry-based and histology-based evaluation was not unique to the *Cd44* gene but was also for a number of other tested genes, such as *Thbd*, which showed downregulation in flow cytometry but not in histology (Figures S3A and S3B). Interestingly, most of the *CD44*$^+$ subset of *CD31*$^+$/*CD45*$^-$ cells were *THBD*$^-$ (Figure S3A), suggesting that the *CD44*$^+$ subset in metastases represents a distinct cellular population. Indeed, when backgated to the live-cell gate, the *CD44*$^+$ appeared to cluster differently from the *CD44*$^-$ subset, with slightly less CD31 and slightly more CD45 staining intensities (Figure S4A).

CD31$^+$/*CD45*$^-$/*CD44*$^+$ Cells Associated with Lung Metastases Originate from the *CD45*$^+$ Hematopoietic Lineage in the BM

Next, we set out to determine whether the distinct CD31^{intermediate}/CD45^{dim}/*CD44*$^+$ (CD31^{int}/CD45^{dim}/*CD44*$^+$) population that was also labeled by the Cdh5-tdT reporter (Figure 1B) represents tumor EC heterogeneity (Dudley, 2012) or a yet-unidentified population in the TME. First, we examined two additional parameters commonly used for determining EC identity, VE-cadherin antibody staining, and tomato lectin binding (Baluk and McDonald, 2008; Gao et al., 2008). VE-cadherin antibody staining in flow cytometry may underestimate the true number

(B) WT or Cdh5-tdT mice were i.v. injected with E0771-LG cells or untreated, and the lungs were analyzed after 11 days.
(C) The gated cells from (A) were prepared for RNA sequencing. The gene expression data were analyzed using unsupervised hierarchical clustering, with bars indicating individual samples.
(D) Independent qRT-PCR validation of *Cd44*. Ct, threshold cycle.
(E) Experimental metastases induced by E0771-LG i.v. injection were analyzed for CD44 expression in the *CD31*$^+$/*CD45*$^-$ population.
(F) Spontaneous lung metastases developed in 14.5-week-old PyMT mice were similarly analyzed.
(G–T) Normal lungs (G and K) or lungs bearing E0771-LG-Luc-ZsGreen (green) metastases (L–T) were sectioned and stained for CD31, CD44, and DAPI for confocal imaging, as presented in xy, xz, and yz views. Yellow arrows indicate *CD31*$^+$ ECs that do not express CD44, and yellow arrowheads indicate the rare occasions in which *CD31*$^+$ ECs appear to express CD44. Orange and blue squares in (K) and (P) are zoomed in panels as indicated. Scale bars, 20 μm.
(U) Quantification of *CD31*$^+$ cells for CD44 positivity. Error bars represent SEM
See also Figures S1–S3.

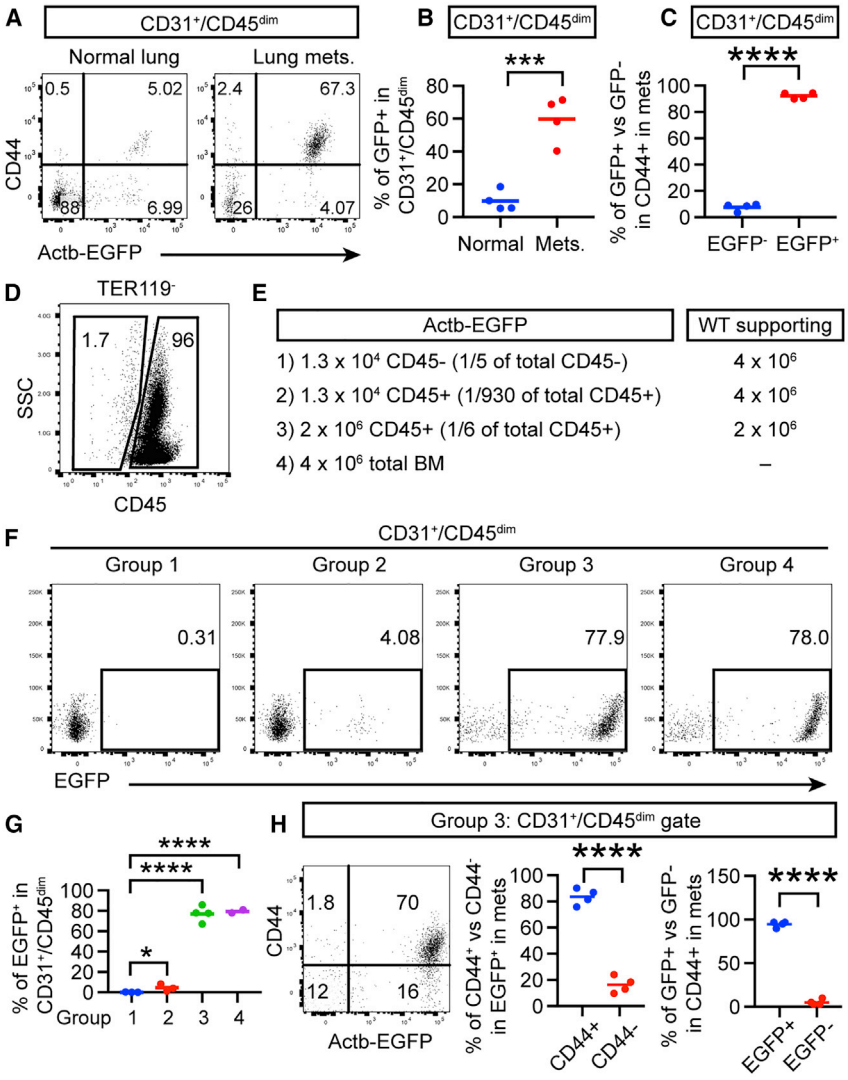

Figure 2. *CD31*$^+$/*CD45*$^-$/*CD44*$^+$ Cells Enriched in Lung Metastases Originate from the *CD45*$^+$ Hematopoietic Lineage in the BM

(A–C) Total BM cells from Actb-EGFP donor mice were transplanted into WT recipient mice. After 5 weeks, E0771-LG cells were injected i.v., and the normal lungs without tumor cell injection or lung metastases were analyzed.

(D–G) The CD45$^-$/TER119$^-$ and CD45$^+$/TER119$^-$ populations were sorted from the total BM cells of Actb-EGFP donor mice and were combined with or without WT supporting cells as indicated for transplantation of WT recipient mice. E0771-LG cells were injected i.v. 5 weeks after transplantation.

(H) Analysis of group 3 in (E) for CD44 and EGFP.

of positive cells (66.3% of *CD31*$^+$/*CD45*$^-$, Figure S4B), possibly due to tissue digestion needed for single-cell preparation. Nevertheless, CD31^{int}/CD45^{dim}/*CD44*$^+$ cells in lung metastases still expressed a significant level of VE-cadherin, in contrast to the 1.9% of *CD45*$^+$ cells as a negative control (Figure S4B, Q1/(Q1+Q2)). 92% of CD31^{int}/CD45^{dim}/CD44$^+$ cells in lung metastases were labeled with lectin after i.v. injection (Figure S4C, Q1/(Q1+Q2)). *Cdh5-tdT* reporter mice also confirmed that most of CD31^{int}/CD45^{dim}/*CD44*$^+$ cells in lung metastases were positive for the reporter (Figure S4D, Q1/(Q1+Q2)). Thus, flow cytometric analysis with conventional EC markers cannot exclude their EC identity.

We then studied the possible involvement of *CD31*$^+$ cells that are not ECs. We excluded the possibility of tumor cell contamination due to vasculogenic mimicry, by which tumor cells express CD31 and become part of the endothelium (Seftor et al., 2012), as *ZsGreen*$^+$ tumor cells were negative for CD31 staining in both histology and flow cytometry (Figures 1L–1T; Figure S4E). They are unlikely to be CD31-expressing monocytic cells either (Kim et al., 2009; Urbich et al., 2003), since, in addition to the relative absence of the pan-leukocyte marker CD45, the myeloid cell marker CD11B expressed by monocytic cells was also negative (Figure S4F).

BM-derived EPCs have been suggested as a source for *CD31*$^+$ cells in tumors (Bertolini et al., 2006; Patenaude et al., 2010). We reasoned that, if the *CD44*$^+$ subset of *CD31*$^+$/*CD45*$^-$ cells originates from EPCs in the BM, they would be labeled in a BM transplantation (BMT) experiment using a colored reporter. Thus, we transplanted total BM cells from *Actb-EGFP* mice (EGFP expression driven by the beta-actin promoter) (Okabe et al., 1997) into wild-type (WT) recipient mice so that BM-derived cells but not pre-existing ECs in lung vessels would be labeled with EGFP. Similar to a previous finding (Gao et al., 2008), the percentage of BM-derived cells in the *CD31*$^+$/*CD45*$^-$ population was significantly increased in lung metastases compared to that in normal lungs (Figures 2A and 2B). Importantly, the majority of *CD44*$^+$ cells that increased in the *CD31*$^+$/*CD45*$^-$ population in lung metastases were *EGFP*$^+$ (Figure 2C), indicating that BM is the source of these cells. Putative EPCs has been postulated to be *CD45*$^-$ non-hematopoietic progenitors in the BM (Gao et al., 2008; Patenaude et al., 2010). However, formal experimental proof for this hypothesis is lacking. To determine whether EPCs by this definition is the cell of origin of our observed CD31^{int}/CD45^{dim}/*CD44*$^+$ cells in lung metastases, we FACS-sorted non-hematopoietic cells (*CD45*$^-$/*TER119*$^-$) and hematopoietic cells not including erythrocytes (*CD45*$^+$/*TER119*$^-$) from the BM and compared their ability to generate CD31^{int}/CD45^{dim}/*EGFP*$^+$ cells in lung metastases after BMT (Figures 2D and 2E). The result showed that only progenitors of the hematopoietic lineage (*CD45*$^+$/*TER119*$^-$) gave rise to *CD31*$^+$/*CD45*$^-$ cells (of which most were *CD44*$^+$) in a dose-dependent manner, and, when given at a similar dose, *CD45*$^+$ engraftment was similarly efficient as total BM cells, in contrast to the undetectable level engrafted by non-hematopoietic *CD45*$^-$ cells (Figures 2F and 2G). In addition, the majority of

CD31^{+}/CD45^{dim}/*CD44*$^{+}$ cells originated from *CD45*$^{+}$ BM progenitors (Figure 2H). Thus, it can be concluded that it is *CD45*$^{+}$ hematopoietic progenitor cells in the BM that give rise to metastasis-infiltrating CD31^{int} cells that are CD45^{dim}.

CD31^{int}/CD45^{dim}/*CD44*$^{+}$ Cells Accumulated in Lung Metastases Are Large Platelets

Next, we studied how *CD45*$^{+}$ hematopoietic progenitors generated CD31^{int}/*CD44*$^{+}$ cells in lung metastases that were CD45^{dim}. We ruled out that they are *CD45*$^{-}$ erythrocytes in metastases, as they were negative for the lineage marker TER119 (Figure S4G). Platelets also express CD31 and are another subset of hematopoietic cells without CD45 expression (Newman and Newman, 2003). Indeed, we found that CD31^{int}/CD45^{dim}/*CD44*$^{+}$ cells in lung metastases were predominantly positive for the platelet marker CD41 (Figures 3A and 3B). Nuclear staining by Hoechst (Hst) confirmed that these cells did not have nuclear DNA (Figures 3C and 3D). Similar results were observed in the spontaneous model (Figure 3E). Next, we FACS-sorted these cells and plated them on a glass slide for fluorescent microscopy. As expected, *CD31*$^{+}$/*CD45*$^{-}$ from the normal lung were positive for CD31 and nuclear staining, while the *CD31*$^{-}$/*CD45*$^{+}$ leukocytes, despite their nuclear staining by Hst, were *CD31*$^{-}$ (Figure 3F, left two columns). In comparison, while the CD31^{int}/CD45^{dim}/*CD44*$^{-}$/*Hst*$^{+}$ cells sorted from metastases appeared to represent authentic ECs due to positive staining for both CD31 and Hst, the *CD44*$^{+}$/*Hst*$^{-}$ subset did not show nuclear staining despite their CD31 staining (Figure 3F, right two column). These cells therefore appeared to be platelets.

To further confirm the platelet identity, we used a reporter mouse in which tdTomato expression is controlled by the MK/platelet lineage marker *Pf4*, *Pf4-tdT* (Madisen et al., 2010; Tiedt et al., 2007). Whereas mice without tumor cell injection showed little PF4-tdT signal in *CD31*$^{+}$/CD45^{dim} cells in the lung, a significant fraction of the *CD31*$^{+}$/CD45^{dim} cells in lung metastases highly expressed PF4-tdT (Figures 3G and 3H). Importantly, these *PF4-tdT*$^{+}$ cells were predominantly *CD44*$^{+}$/*CD41*$^{+}$/*Hst*$^{-}$ (Figure 3H), which reinforces the platelet identity of these cells.

Lung Metastases but Not Primary Tumors Induce Accumulation of Chemokine-Expressing CD31^{int}/CD45^{dim}/*CD44*$^{+}$ Large Platelets

To examine whether CD31^{int}/CD45^{dim}/*CD44*$^{+}$ platelets exhibit any distinct features compared to regular platelets, we compared their sizes and CD44 expression and found that CD31^{int}/CD45^{dim}/*CD44*$^{+}$ were larger and that only these cells express CD44 (Figure 4A). Next, we tested whether CD31^{int}/CD45^{dim}/*CD44*$^{+}$ large platelets exist in the blood circulation before they were recruited to lung metastases or even in the blood of normal mice. Indeed, we found CD31^{int}/CD45^{dim} cells in the normal blood as described also by others (Strijbos et al., 2007; Wong et al., 2012) and that these cells were *CD44*$^{+}$/*CD41*$^{+}$/*Hst*$^{-}$ (Figure 4B, P1). However, the number of CD31^{int}/CD45^{dim}/*CD44*$^{+}$ cells did not increase in the blood of metastasis-bearing mice (Figure 4C), despite their marked increase in lung metastases (Figure 1E), suggesting local production in the lung.

Subsequently, we wanted to understand whether CD31^{int}/CD45^{dim}/*CD44*$^{+}$ large platelets enriched in lung metastases express chemokines that may regulate recruitment and function of myeloid cells and thus metastatic growth indirectly. qRT-PCR analysis of these cells strikingly revealed that only the CD31^{int}/CD45^{dim}/*CD44*$^{+}$ large platelets accumulated in lung metastases highly expressed a number of chemokines identified in the RNA-seq, such as *Cxcl2*, *Cxcl10*, *Cxcl1*, *Cxcl3*, and *Ccl2* data (Table S1, tabs "Pathways," "Agranulocyte Adhesion and Diapedesis," and "Leukocyte Extravasation Signaling"; Figure 4D). Neither those in the blood of normal mice or metastasis-bearing mice showed detectable levels (Figure 4D). This observation again indicates a local effect in the lung, which prompted us to examine the primary mammary tumors. Notably, very few CD31^{int}/CD45^{dim}/*CD44*$^{+}$ large platelets were detected in MMTV-PyMT primary tumors (Figure 4E), in sharp contrast to the lung metastases in this model (Figure 1F). In comparison, regular small platelets did not show such a lung-preferential enrichment, as they were present in a similar level in primary tumors as in normal mammary fat pads (Figure S5). A recent important finding showed that lung megakaryocytes (MKs) in the BM can egress from the BM and reside in the lung and contribute to platelet production (Lefrançais et al., 2017). Consistent with these data, we observed in lung metastases *Pf4-tdT*$^{+}$ MKs (Figure 4F) that may represent the source of the chemokine-expressing large platelets enriched only in lung metastases. Interestingly, *Pf4-tdT*$^{+}$ MKs in mice that received Pf4-tdT BMT increased in lung metastases (Figure 4F), suggesting that lung metastases may induce MK migration from the BM to the lung or *in situ* proliferation.

DISCUSSION

We initially set out to test whether cancer cells colonizing the lung induce a distinct expression program in associated ECs. To our surprise, we found in this study a previously unrecognized yet distinct population of CD31^{int}/CD45^{dim}/*CD44*$^{+}$large platelets restricted to lung metastases.

Our unexpected findings have helped to clarify the controversial concept of EPCs. It was postulated but not experimentally proved that EPCs are a population of *CD45*$^{-}$ non-hematopoietic progenitors in the BM that are able to generate BM-derived *CD31*$^{+}$/*CD45*$^{-}$ cells in tumors, including lung metastases (Gao et al., 2008; Patenaude et al., 2010). However, our lineage tracing experiments that compared *CD45*$^{+}$ and *CD45*$^{-}$ BM cells for this progenitor ability has provided strong evidence that BM-derived *CD31*$^{+}$/*CD45*$^{-}$ cells, at least in lung metastases, originate from *CD45*$^{+}$ hematopoietic progenitors. This finding argues against the *in vivo* existence of a unique population of EPCs located in the BM that are non-hematopoietic. It should be noted that we do not exclude differentiation into ECs from BM-derived hematopoietic progenitor cells (Moschetta et al., 2014; Patenaude et al., 2010) or from vessel-wall-derived progenitors (Ingram et al., 2005; Fang et al., 2012; Wakabayashi et al., 2018). However, this is not the conventional definition of EPCs that emphasizes the BM origin and the non-hematopoietic identity.

Platelets are released from MKs with an intermediate stage of proplatelets (Patel et al., 2005). The CD31^{int}/CD45^{dim}/*CD44*$^{+}$

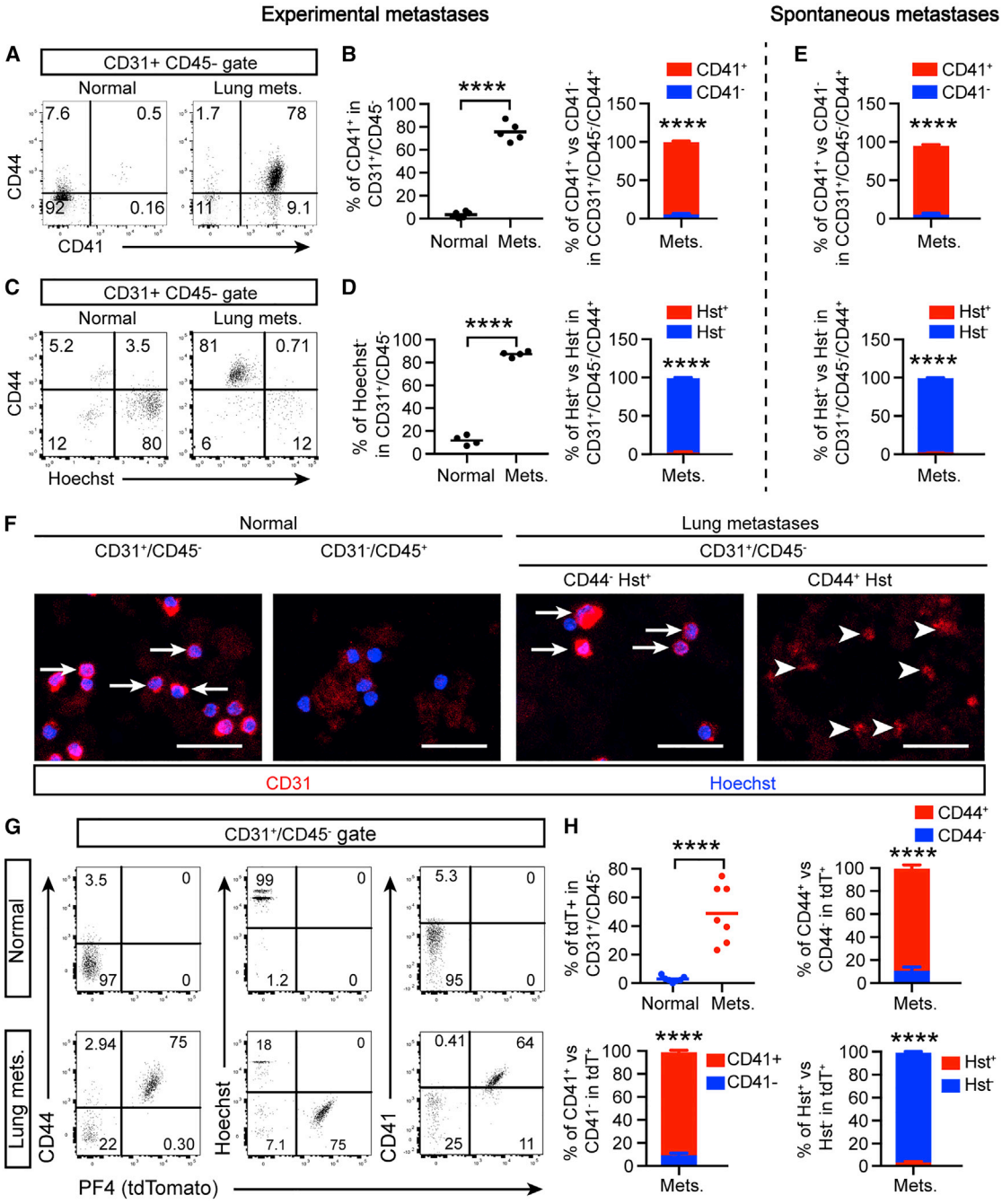

Figure 3. CD31^{int}/CD45^{dim}/*CD44*$^{+}$ Cells Enriched in Lung Metastases Are *CD41*$^{+}$/*Hoechst*$^{-}$/*Pf4*$^{+}$ Platelets

(A–D) Lung metastases induced by E0771-LG i.v. injection were analyzed after 11 days for CD41 expression (A and B) or Hoechst (Hst) staining (C and D).

(E) Lung metastases were dissected from 14.5-week-old PyMT mice for similar analyses.

(F) The indicated cell populations from the experimental metastasis model were sorted and fixed on a glass slide for imaging. Arrows indicate *CD31*$^{+}$/*Hst*$^{+}$ ECs; arrowheads indicate CD31^{+}/*Hst*$^{-}$ platelets. Scale bars, 25 μm.

(G) WT mice that received Pf4-tdT BMT were either untreated or i.v. injected with E0771-LG. After 11 days, the lungs and lung metastases were analyzed.

(H) Quantification of (G). All error bars represent mean ± SEM.

See also Figure S4.

large platelets identified in our study may represent this poorly understood intermediate form. Recently Lefrancais et al. showed that MKs commonly found in the BM can migrate to and reside in the lung, where they contribute up to 50% of the total platelet production (Lefrançais et al., 2017). These lung-resident MKs are likely the source of the CD31^{int}/CD45^{dim}/*CD44*$^{+}$ large

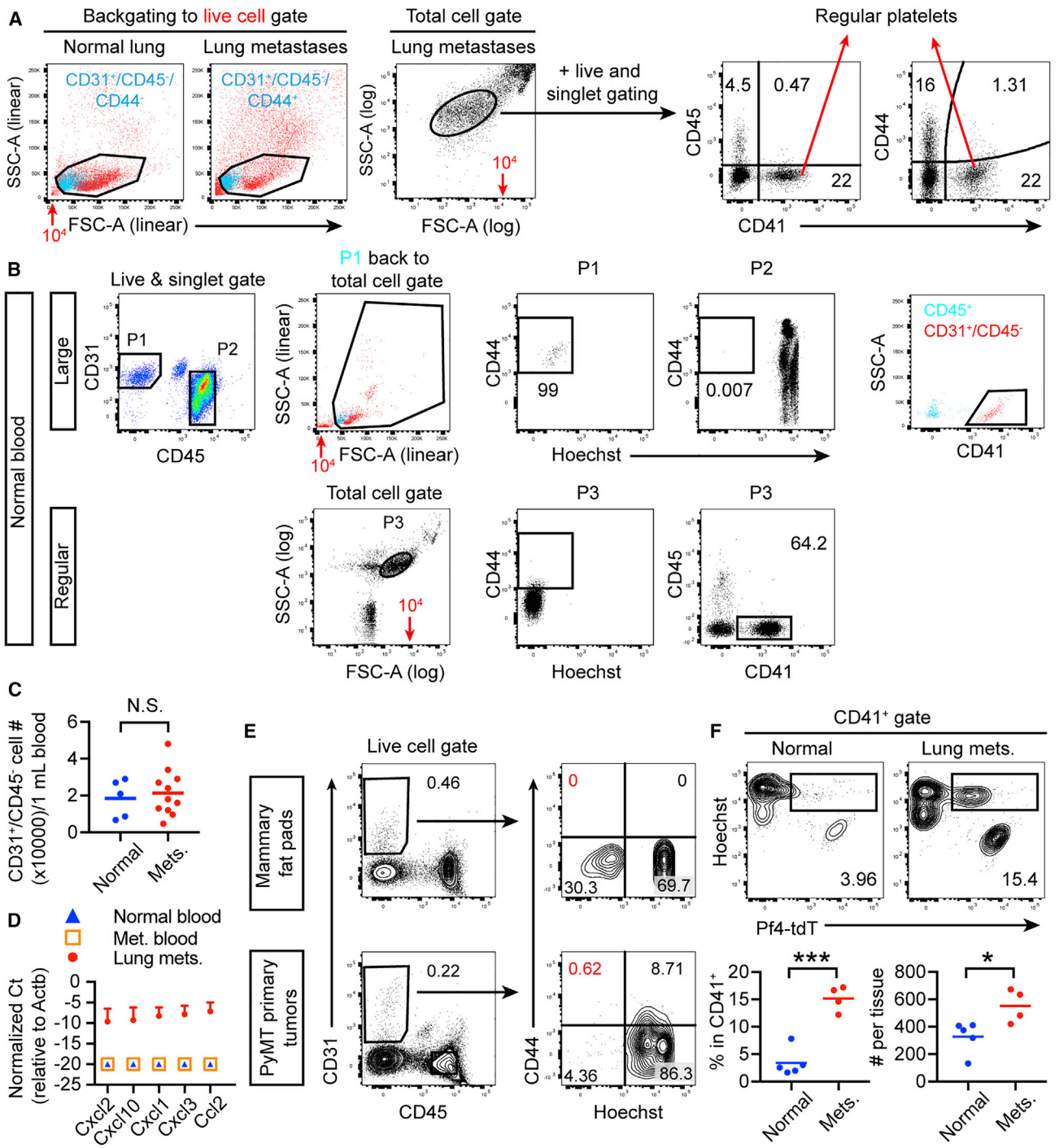

Figure 4. Lung Metastases But Not Primary Tumors Induce Accumulation of Chemokine-Expressing CD31^{int}/CD45^{dim}/*CD44*$^{+}$ Large Platelets

(A and B) Comparison of CD31^{int}/CD45^{dim}/*CD44*$^{+}$ large platelets and regular small platelets in the lung (A) and blood (B). Note the same values of 10^4 (red text and arrows) on different scales of forward scatter (FSC).

(C) Quantification of CD31^{int}/CD45^{dim}/*CD44*$^{+}$ large platelets in the blood of normal and metastasis-bearing mice.

(D) CD31^{int}/CD45^{dim}/*CD44*$^{+}$ large platelets from the normal blood, the blood of metastasis-bearing mice, and dissected lung metastases were sorted for qRT-PCR analysis.

(legend continued on next page)

platelets that are enriched and activated only in lung metastases. Future work such as intravital imaging is required to provide direct evidence of this assertion and to obtain the spatial-temporal information of the multiple cell types in metastases. Nevertheless, our findings have extended the significance of the lung-resident population of MKs by showing that they represent a distinct player that releases chemokine-expressing large platelets to metastatic cancer cells in the lung.

The exact function of CD31^{int}/CD45^{dim}/*CD44*$^{+}$ large platelets requires further study. They may use similar mechanisms as regular small platelets to promote cancer cell extravasation and metastatic growth (Haemmerle et al., 2018), or they may also have distinct roles. For example, only the CD31^{int}/CD45^{dim} large platelets but not regular small ones expressed CD44. Since CD44 binds to HA, and HA deposition by tumor and stromal cells is enhanced upon their interaction (Kimata et al., 1983; Knudson et al., 1984), CD31^{int}/CD45^{dim}/*CD44*$^{+}$ large platelets may use this adhesion mechanism to accumulate in metastases. Elucidation of the specific activities of this population will require advances that allow perturbation of only these atypical platelets but not the regular ones. Unfortunately, unique tools to study this cell population do not exist. Despite the limitations, our observation that lung metastases induced upregulation of chemokines in CD31^{int}/CD45^{dim}/*CD44*$^{+}$ large platelets has shed important mechanistic insights, since many of these chemokines have been shown in a variety of studies to regulate the recruitment and activity of monocytes, macrophages, and neutrophils to promote extravasation, seeding, and colonization of disseminated tumor cells (Coffelt et al., 2016; Kitamura et al., 2015a). Additional future work is needed to determine the amount and functional effects of these chemokines as compared to those from other stromal cells in the TME including regular platelets.

Identification of this platelet population has advanced our understanding of the heterogeneity and complexion of the TME in metastases. Our study suggests that metastatic cancer cells may trigger organ-specific responses. Elucidation of these mechanisms may offer opportunities for design of novel therapeutics.

STAR★METHODS

Detailed methods are provided in the online version of this paper and include the following:

- KEY RESOURCES TABLE
- LEAD CONTACT AND MATERIALS AVAILABILITY
- EXPERIMENTAL MODEL AND SUBJECT DETAILS
  - Animals
  - Cell lines
- METHOD DETAILS
  - Lung metastasis assays
  - Viral production and transduction of tumor cells
  - Flow cytometry and cell sorting
  - BMT
  - RNA isolation, qRT-PCR and RNA sequencing
  - Immunofluorescent staining and microscopy
- QUANTIFICATION AND STATISTICAL ANALYSIS
- DATA AND CODE AVAILABILITY

SUPPLEMENTAL INFORMATION

Supplemental Information can be found online at https://doi.org/10.1016/j.celrep.2019.10.016.

ACKNOWLEDGMENTS

We thank Drs. Shentong Fang, Antonio Di Cristofano, and Donald McDonald for valuable discussion. We acknowledge support from the Flow Cytometry Core Facility (partially supported by NCI P30CA013330) and the Analytical Imaging Facility (funded by NCI P30CA013330). The Leica SP8 confocal microscope was funded by the NIH 1S10OD023591-01. This work was supported by NIH grant P30CA0133330.

AUTHOR CONTRIBUTIONS

W.Z. and J.W.P. conceived and designed the study. W.Z. performed the majority of experiments. H.Z. provided important technical support. D.Z. analyzed the RNA-seq data. J.Z. made intellectual contributions to the platelet study. W.Z. and J.W.P. analyzed and interpreted the data and wrote the manuscript.

DECLARATION OF INTERESTS

The authors declare no competing interests.

Received: December 21, 2018
Revised: September 12, 2019
Accepted: October 3, 2019
Published: November 12, 2019

REFERENCES

Alva, J.A., Zovein, A.C., Monvoisin, A., Murphy, T., Salazar, A., Harvey, N.L., Carmeliet, P., and Iruela-Arispe, M.L. (2006). VE-Cadherin-Cre-recombinase transgenic mouse: a tool for lineage analysis and gene deletion in endothelial cells. Dev. Dyn. *235*, 759–767.

Anders, S., Pyl, P.T., and Huber, W. (2015). HTSeq–a Python framework to work with high-throughput sequencing data. Bioinformatics *31*, 166–169.

Baluk, P., and McDonald, D.M. (2008). Markers for microscopic imaging of lymphangiogenesis and angiogenesis. Ann. N Y Acad. Sci. *1131*, 1–12.

Bertolini, F., Shaked, Y., Mancuso, P., and Kerbel, R.S. (2006). The multifaceted circulating endothelial cell in cancer: towards marker and target identification. Nat. Rev. Cancer *6*, 835–845.

Butler, J.M., Nolan, D.J., Vertes, E.L., Varnum-Finney, B., Kobayashi, H., Hooper, A.T., Seandel, M., Shido, K., White, I.A., Kobayashi, M., et al. (2010). Endothelial cells are essential for the self-renewal and repopulation of Notch-dependent hematopoietic stem cells. Cell Stem Cell *6*, 251–264.

Coffelt, S.B., Wellenstein, M.D., and de Visser, K.E. (2016). Neutrophils in cancer: neutral no more. Nat. Rev. Cancer *16*, 431–446.

Dudley, A.C. (2012). Tumor endothelial cells. Cold Spring Harb. Perspect. Med. *2*, a006536.

(E) Primary tumors from 13-week-old MMTV-PyMT mice and normal mammary fat pads from WT littermates were analyzed. The red percentages indicate the essential absence of *CD44*$^{+}$/*Hoechst*$^{-}$ cells.

(F) WT mice that received Pf4-tdT BMT were injected i.v. with E0771-LG, and the lungs and lung metastases were analyzed after 11 days. *tdT*$^{+}$/*Hst*$^{+}$ cells are quantified as percentage of *CD41*$^{+}$ cells and absolute numbers.

See also Figure S5.

Fang, S., Wei, J., Pentinmikko, N., Leinonen, H., and Salven, P. (2012). Generation of functional blood vessels from a single c-kit+ adult vascular endothelial stem cell. PLoS Biol. *10*, e1001407.

Favre, C.J., Mancuso, M., Maas, K., McLean, J.W., Baluk, P., and McDonald, D.M. (2003). Expression of genes involved in vascular development and angiogenesis in endothelial cells of adult lung. Am. J. Physiol. Heart Circ. Physiol. *285*, H1917–H1938.

Gao, D., Nolan, D.J., Mellick, A.S., Bambino, K., McDonnell, K., and Mittal, V. (2008). Endothelial progenitor cells control the angiogenic switch in mouse lung metastasis. Science *319*, 195–198.

Gil-Bernabé, A.M., Ferjancic, S., Tlalka, M., Zhao, L., Allen, P.D., Im, J.H., Watson, K., Hill, S.A., Amirkhosravi, A., Francis, J.L., et al. (2012). Recruitment of monocytes/macrophages by tissue factor-mediated coagulation is essential for metastatic cell survival and premetastatic niche establishment in mice. Blood *119*, 3164–3175.

Grivennikov, S.I., Greten, F.R., and Karin, M. (2010). Immunity, inflammation, and cancer. Cell *140*, 883–899.

Guy, C.T., Cardiff, R.D., and Muller, W.J. (1992). Induction of mammary tumors by expression of polyomavirus middle T oncogene: a transgenic mouse model for metastatic disease. Mol. Cell. Biol. *12*, 954–961.

Haemmerle, M., Stone, R.L., Menter, D.G., Afshar-Kharghan, V., and Sood, A.K. (2018). The Platelet Lifeline to Cancer: Challenges and Opportunities. Cancer Cell *33*, 965–983.

Ingram, D.A., Mead, L.E., Moore, D.B., Woodard, W., Fenoglio, A., and Yoder, M.C. (2005). Vessel wall-derived endothelial cells rapidly proliferate because they contain a complete hierarchy of endothelial progenitor cells. Blood *105*, 2783–2786.

Kim, S.J., Kim, J.-S., Papadopoulos, J., Wook Kim, S., Maya, M., Zhang, F., He, J., Fan, D., Langley, R., and Fidler, I.J. (2009). Circulating monocytes expressing CD31: implications for acute and chronic angiogenesis. Am. J. Pathol. *174*, 1972–1980.

Kim, D., Pertea, G., Trapnell, C., Pimentel, H., Kelley, R., and Salzberg, S.L. (2013). TopHat2: accurate alignment of transcriptomes in the presence of insertions, deletions and gene fusions. Genome Biol. *14*, R36.

Kimata, K., Honma, Y., Okayama, M., Oguri, K., Hozumi, M., and Suzuki, S. (1983). Increased synthesis of hyaluronic acid by mouse mammary carcinoma cell variants with high metastatic potential. Cancer Res. *43*, 1347–1354.

Kitamura, T., Qian, B.-Z., and Pollard, J.W. (2015a). Immune cell promotion of metastasis. Nat. Rev. Immunol. *15*, 73–86.

Kitamura, T., Qian, B.-Z., Soong, D., Cassetta, L., Noy, R., Sugano, G., Kato, Y., Li, J., and Pollard, J.W. (2015b). CCL2-induced chemokine cascade promotes breast cancer metastasis by enhancing retention of metastasis-associated macrophages. J. Exp. Med. *212*, 1043–1059.

Knudson, W., Biswas, C., and Toole, B.P. (1984). Interactions between human tumor cells and fibroblasts stimulate hyaluronate synthesis. Proc. Natl. Acad. Sci. USA *81*, 6767–6771.

Lefrançais, E., Ortiz-Muñoz, G., Caudrillier, A., Mallavia, B., Liu, F., Sayah, D.M., Thornton, E.E., Headley, M.B., David, T., Coughlin, S.R., et al. (2017). The lung is a site of platelet biogenesis and a reservoir for haematopoietic progenitors. Nature *544*, 105–109.

Lertkiatmongkol, P., Liao, D., Mei, H., Hu, Y., and Newman, P.J. (2016). Endothelial functions of platelet/endothelial cell adhesion molecule-1 (CD31). Curr. Opin. Hematol. *23*, 253–259.

Lin, E.Y., Jones, J.G., Li, P., Zhu, L., Whitney, K.D., Muller, W.J., and Pollard, J.W. (2003). Progression to malignancy in the polyoma middle T oncoprotein mouse breast cancer model provides a reliable model for human diseases. Am. J. Pathol. *163*, 2113–2126.

Love, M.I., Huber, W., and Anders, S. (2014). Moderated estimation of fold change and dispersion for RNA-seq data with DESeq2. Genome Biol. *15*, 550.

Madisen, L., Zwingman, T.A., Sunkin, S.M., Oh, S.W., Zariwala, H.A., Gu, H., Ng, L.L., Palmiter, R.D., Hawrylycz, M.J., Jones, A.R., et al. (2010). A robust and high-throughput Cre reporting and characterization system for the whole mouse brain. Nat. Neurosci. *13*, 133–140.

Medina, R.J., Barber, C.L., Sabatier, F., Dignat-George, F., Melero-Martin, J.M., Khosrotehrani, K., Ohneda, O., Randi, A.M., Chan, J.K.Y., Yamaguchi, T., et al. (2017). Endothelial Progenitors: A Consensus Statement on Nomenclature. Stem Cells Transl. Med. *6*, 1316–1320.

Moschetta, M., Mishima, Y., Sahin, I., Manier, S., Glavey, S., Vacca, A., Roccaro, A.M., and Ghobrial, I.M. (2014). Role of endothelial progenitor cells in cancer progression. Biochim. Biophys. Acta *1846*, 26–39.

Newman, P.J., and Newman, D.K. (2003). Signal transduction pathways mediated by PECAM-1: new roles for an old molecule in platelet and vascular cell biology. Arterioscler. Thromb. Vasc. Biol. *23*, 953–964.

Okabe, M., Ikawa, M., Kominami, K., Nakanishi, T., and Nishimune, Y. (1997). 'Green mice' as a source of ubiquitous green cells. FEBS Lett. *407*, 313–319.

Orian-Rousseau, V., and Ponta, H. (2015). Perspectives of CD44 targeting therapies. Arch. Toxicol. *89*, 3–14.

Patel, S.R., Hartwig, J.H., and Italiano, J.E., Jr. (2005). The biogenesis of platelets from megakaryocyte proplatelets. J. Clin. Invest. *115*, 3348–3354.

Patenaude, A., Parker, J., and Karsan, A. (2010). Involvement of endothelial progenitor cells in tumor vascularization. Microvasc. Res. *79*, 217–223.

Potente, M., Gerhardt, H., and Carmeliet, P. (2011). Basic and therapeutic aspects of angiogenesis. Cell *146*, 873–887.

Powell, D.R., and Huttenlocher, A. (2016). Neutrophils in the Tumor Microenvironment. Trends Immunol. *37*, 41–52.

Seftor, R.E.B., Hess, A.R., Seftor, E.A., Kirschmann, D.A., Hardy, K.M., Margaryan, N.V., and Hendrix, M.J.C. (2012). Tumor cell vasculogenic mimicry: from controversy to therapeutic promise. Am. J. Pathol. *181*, 1115–1125.

Steeg, P.S. (2016). Targeting metastasis. Nat. Rev. Cancer *16*, 201–218.

Strijbos, M.H., Kraan, J., den Bakker, M.A., Lambrecht, B.N., Sleijfer, S., and Gratama, J.W. (2007). Cells meeting our immunophenotypic criteria of endothelial cells are large platelets. Cytometry B Clin. Cytom. *72*, 86–93.

Tiedt, R., Schomber, T., Hao-Shen, H., and Skoda, R.C. (2007). Pf4-Cre transgenic mice allow the generation of lineage-restricted gene knockouts for studying megakaryocyte and platelet function in vivo. Blood *109*, 1503–1506.

Trapnell, C., Hendrickson, D.G., Sauvageau, M., Goff, L., Rinn, J.L., and Pachter, L. (2013). Differential analysis of gene regulation at transcript resolution with RNA-seq. Nat. Biotechnol. *31*, 46–53.

Urbich, C., Heeschen, C., Aicher, A., Dernbach, E., Zeiher, A.M., and Dimmeler, S. (2003). Relevance of monocytic features for neovascularization capacity of circulating endothelial progenitor cells. Circulation *108*, 2511–2516.

Wakabayashi, T., Naito, H., Suehiro, J.I., Lin, Y., Kawaji, H., Iba, T., Kouno, T., Ishikawa-Kato, S., Furuno, M., Takara, K., et al. (2018). CD157 Marks Tissue-Resident Endothelial Stem Cells with Homeostatic and Regenerative Properties. Cell Stem Cell *22*, 384–397.

Wong, C.K.E., Namdarian, B., Chua, J., Chin, X., Speirs, R., Nguyen, T., Fankhauser, M., Pedersen, J., Costello, A.J., Corcoran, N.M., and Hovens, C.M. (2012). Levels of a subpopulation of platelets, but not circulating endothelial cells, predict early treatment failure in prostate cancer patients after prostatectomy. Br. J. Cancer *107*, 1564–1573.

STAR★METHODS

KEY RESOURCES TABLE

REAGENT or RESOURCE	SOURCE	IDENTIFIER
Antibodies		
CD11B, PE-Cy7, clone M1/70	BioLegend	Cat# 101215, RRID:AB_312798
CD11B, PE, clone M1/70	BD Biosciences	Cat# 561689, RRID:AB_10893803
CD31, clone MAB1398Z	Millipore	Cat# MAB1398Z, RRID:AB_94207
CD31, clone MEC13.3	BD Biosciences	Cat# 550274, RRID:AB_393571
CD31, BV421, clone 390	BD Biosciences	Cat# 563356, RRID:AB_2738154
CD31, AF647, clone 390	BD Biosciences	Cat# 563608, RRID:AB_2738313
CD44, clone IM7	BD Biosciences	Cat# 553131, RRID:AB_394646
CD41, BUV395, clone MWReg30	BD Biosciences	Cat# 565980, RRID:AB_2739432
CD41, PE, clone MWReg30	BD Biosciences	Cat# 561850, RRID:AB_10896980
CD44, FITC, clone IM7	BioLegend	Cat# 103021, RRID:AB_493684
CD44, PE-Cy7, clone IM7	BioLegend	Cat# 103030, RRID:AB_830787
CD45, PerCP-Cy5.5, clone 30-F11	BD Biosciences	Cat# 550994, RRID:AB_394003
CD45, APC, clone 30-F11	BD Biosciences	Cat# 559864, RRID:AB_398672
Donkey anti-rat, AF488	ThermoFisher	Cat# A-21208, RRID:AB_2535794
Donkey anti-rat, AF594	ThermoFisher	Cat# A-21209, RRID:AB_2535795
Goat anti-hamster, AF647	Jackson ImmunoResearch	127-605-160, RRID:AB_2339001
Goat anti-hamster, AF488	Jackson ImmunoResearch	Cat# 127-545-160, RRID:AB_2338997
Streptavidin BUV395	BD Biosciences	Cat# 564176
TER119, PE-Cy7, clone TER-119	BD Biosciences	Cat# 557853, RRID:AB_396898
THBD, PE, clone LS17-9	BD Biosciences	Cat# 566338, RRID:AB_2739695
THBD	R&D	Cat# AF3894, RRID: AB_664141
VE-cadherin, APC, clone 11D4.1	BD Biosciences	Cat# 562242
Chemicals, Peptides, and Recombinant Proteins		
Liberase DL	Sigma-Aldrich	5466202001
Liberase TL	Sigma-Aldrich	5401020001
Hoechst 33342	BD Biosciences	561908
Histopaque 1083	Sigma-Aldrich	1083-1
Deposited Data		
RNA sequencing	This paper	GEO: GSE123520
Experimental Models: Cell Lines		
E0771-LG	Jeffrey Pollard lab (Kitamura et al., 2015b)	N/A
E0771-LG-luciferase-ZsGreen	This paper	N/A
Experimental Models: Organisms/Strains		
Actb-EGFP	Jackson Laboratory	006567
C57/Bl/6J	Jackson Laboratory	C57/Bl/6J
Cdh5-Cre	Jackson Laboratory	006137
MMTV-PyMT	William Muller Lab (Guy et al., 1992)	
Pf4-Cre	Jackson Laboratory	008535
Rosa26-loxp-stop-loxp-tdTomato	Jackson Laboratory	007914
Oligonucleotides		
Actb	ThermoFisher	Mm02619580_g1
Ccl2	ThermoFisher	Mm00441242_m1
Cd44	ThermoFisher	Mm01277161_m1
Cxcl1	ThermoFisher	Mm04207460_m1

(*Continued on next page*)

Continued

REAGENT or RESOURCE	SOURCE	IDENTIFIER
Cxcl10	ThermoFisher	Mm00445235_m1
Cxcl2	ThermoFisher	Mm00436450_m1
Cxcl3	ThermoFisher	Mm01701838_m1
Recombinant DNA		
pHIV-Luc-ZsGreen	Bryan Welm Lab	Addgene 39196
pMD2.G	Didier Trono	Addgene 12259
psPAX2	Didier Trono	Addgene 12260
Software and Algorithms		
ImageJ	NIH	https://imagej.nih.gov/ij/
Prism 7.0	GraphPad Software	https://www.graphpad.com/
FlowJo	FlowJo	https://www.flowjo.com/
Ingenuity Pathway Analysis	Ingenuity System Inc	https://www.ingenuity.com/
Tophat v2.0.13	Kim et al., 2013	https://ccb.jhu.edu/software/tophat/index.shtml
HTSeq v0.6.1	Anders et al., 2015	https://htseq.readthedocs.io/en/release_0.10.0/overview.html
DESeq2 v1.6.3	Love et al., 2014	https://bioconductor.org/packages/release/bioc/html/DESeq2.html
Cufflinks v2.2.1	Trapnell et al., 2013	http://cole-trapnell-lab.github.io/cufflinks/manual/

LEAD CONTACT AND MATERIALS AVAILABILITY

Further information and requests for resources and reagents should be directed to and will be fulfilled by the Lead Contact, Jeffrey Pollard (jeffrey.pollard@einstein.yu.edu). The stable cell line generated in this study will be made available on request, but we may require a payment and/or a completed Materials Transfer Agreement if there is potential for commercial application.

EXPERIMENTAL MODEL AND SUBJECT DETAILS

Animals

All procedures involving mice were conducted in accordance with National Institutes of Health regulations concerning the use and care of experimental animals and were approved by the Albert Einstein College of Medicine Animal Use Committee. MMTV-PyMT mice were provided by W.J. Muller (McMaster University, Hamilton, Ontario, Canada) (Guy et al., 1992) and bred in house in the FVB background. *Cdh5-Cre* (Stock number 006137), *Rosa26-LSL-tdTomato* (Stock number 007914), *Actb-EGFP* (Stock number 006567), *Pf4-Cre* (Stock number 008535) and C57BL6/J WT mice were purchased from the Jackson Laboratory. Only female mice were used in breast cancer models.

Cell lines

E0771-LG (Kitamura et al., 2015b) and 293T cells were cultured in DMEM supplemented with 10% v/v fetal bovine serum and penicillin/streptomycin.

METHOD DETAILS

Lung metastasis assays

Spontaneous metastases in the lung developed in MMTV-PyMT mice were collected when mice were 14-15 weeks old. For experimental metastasis assays, 1×10^6 E0771-LG were injected intravenously through the tail vein of syngenic C57BL6/J female mice (6-8 wk old unless otherwise specified). For *in vivo* analysis of lectin binding, 50μg biotinylated tomato-lectin (Vector Lab, B-1175) was injected into the retro-orbital sinus and was analyzed 10 min after injection by staining with streptavidin-conjugated BUV395 (BD Biosciences 564176).

Viral production and transduction of tumor cells

293T cells were transfected with pHIV-Luc-ZsGreen (gift from Dr. Bryan Welm, Addgene #39196), pMD2.G (gift from Dr. Didier Trono, Addgene #12259) and pxPAX2 (gift from Dr. Didier Trono, Addgene #12260) at 4:3:1 in μg using Lipofectamien 2000 (Invitrogen, #11668-019) according to the manufacturer's manual. Medium was replaced 4-6 hours (h) after transfection with DMEM containing

2% v/v FBS. Viral supernatants were collected 48 and 72 h after transfection, pooled, cleared with a 0.2 μm filter and used for transduction. Target cells were seeded at about 50% confluency, incubated with the viral supernatant and 10 μg/mL polybrene (Santa Cruz, sc-134220) and centrifuged at 1000 G for 30 min at room temperature (RT). The virus was removed and the cells were then cultured for 3 days before FACS sorting for ZsGreen+ cells.

Flow cytometry and cell sorting

Lungs were perfused with PBS through the right ventricle, dissected and minced. Lung metastases (< 1 mm in diameter) were dissected using a dissection microscope and pooled from 2-4 mice. The tissues were then digested with an enzyme mix of Liberase DL (Sigma-Aldrich 5466202001, 0.52 U/mL), TL (Sigma-Aldrich 5401020001, 0.26 U/mL) and DNase I (Sigma-Aldrich DN25, 150 μg/mL) diluted in basal DMEM medium with rotation for 30 min at 37°C and filtered (70-μm membrane). For cells sorted for qRT-PCR, transcription inhibitors alpha-amanitin (Sigma-Aldrich A2263, 5 μg/mL) and actinomycin D (Sigma-Aldrich A1410, 1 μg/mL) were also added in the digestion buffer. Mouse peripheral blood was collected from the major abdominal vessels (inferior vena cava) with a syringe containing 150 μL ACD buffer [85 mM trisodium citrate, 71 mM citric acid, and 111 mM dextrose (pH 4.5)] (Gil-Bernabé et al., 2012). Red blood cells were removed by incubation with the RBC Lysis Buffer (Biolegend, 420301) for 5 min on ice (once for tissues and twice for blood). Before antibody labeling, cells were blocked with anti-mouse CD16/CD32 antibody (BD Biosciences 553141) for 10 min on ice. Flow cytometry was performed with a LSRII cytometer (BD Biosciences) and the data were analyzed using Flowjo software (TreeStar). FACSAria II (BD Biosciences) and Moflo Astrios (Beckman Coulter) were used for cell sorting.

Gating of single cells using FSC-A/H and SSC-A/W and exclusion of dead cells with DAPI, Zombie Yellow (Biolegend 423103) or Zombie Green (Biolegend 423111) staining were performed routinely during analysis. For Hoechst staining, cells were incubated with 5 μg/mL Hoechst 33342 (BD Biosciences, 561908) for 10 min at 37°C before antibody staining. For visualization of sorted cells on a glass slide for microscopy, the sorted cells were pelleted, resuspended in 10 μL PBS, pipetted to a glass slide enclosed by a hydrophobic pen (Vector Laboratories, H-4000) and air-dried in a laminar hood. The cells were then fixed with 4% w/v paraformaldehyde (PFA) for 10 min at room temperature and mounted with VECTASHIELD Mounting Medium (Vector Laboratories, H-1000). For quantification of cell numbers, CountBrignt abosolute counting beads (ThermoFisher Scientific, Cat# C36950) were used according to the manual.

BMT

Total BM cells were extracted from femurs, tibiae and the spine by grinding in a mortar. For BMT involving cell sorting, an additional step was performed to purify low-density mononuclear cells by using density gradient centrifugation with Histopaque 1083 (Sigma-Aldrich 1083-1) before antibody staining. Female recipient mice of 4-6 weeks old were irradiated with 10 Gy gamma rays (split into 2 doses with a 4-h interval) the day before iv injection of 5-10 × 10^6 BM cells unless otherwise specified. Transplanted mice were used for experiments after 4-5 weeks.

RNA isolation, qRT-PCR and RNA sequencing

Cells were sorted directly into the Extraction Buffer of the Picopure RNA Isolation kit (Arcturus KIT0202). RNA sequencing of mouse total RNA was performed at Beijing Genomic Institute, using the Ovation® RNA-Seq System V2 kit for library construction, pair-end 100 bp and Hiseq 4000, which generated 60-80M reads per sample. The reads were aligned to the mouse reference genome (GRCm38/mm10) using Tophat (v2.0.13) (Kim et al., 2013). Uniquely mapped reads were counted for each gene using htseq-count in the HTSeq package (v0.6.1) with gene models from UCSC RefGene (Anders et al., 2015). FPKM values were generated using cuffflinks v2.2.1 (Trapnell et al., 2013). Lowly expressed genes (mean FPKM values < 1 in both groups under comparison) were excluded from differential expression analysis. DESeq2 was used to identify differentially expressed genes (Love et al., 2014), of which fulfilling the following criteria were used for enrichment of Canonical Pathways in the Ingenuity Pathway Analysis (QIAGEN): log2 (fold change) > 1.5; false discovery rate (FDR) < 0.03; for upregulated genes, mean FPKMs of lung metastases > 20; for downregulated genes, mean FPKMs of normal lungs > 20.

For qRT-PCR, the isolated RNAs were reverse transcribed and amplified using QuantiTect® Whole Transcriptome (QIAGEN 207043) before qPCR. Gene expression was normalized to *beta-actin*. Relative expression is calculated using the formula $-\Delta\Delta Ct$, where Ct stands for threshold cycles. Undetectable expressions were assigned a relative Ct value of −20 with respect to the Ct of *beta-actin*. The following Taqman gene expression assays (ThermoFisher Scientific) were used: *Actb* (Mm02619580_g1), *Ccl2* (Mm00441242_m1), *Cd44* (Mm01277161_m1), *Cxcl1* (Mm04207460_m1), *Cxcl2* (Mm00436450_m1), *Cxcl3* (Mm01701838_m1), and *Cxcl10* (Mm00445235_m1).

Immunofluorescent staining and microscopy

Mouse lungs were processed for frozen sectioning using a method modified from a previous study (Favre et al., 2003). Briefly, the lung were perfused with 1% w/v PFA through the right ventricle, and then 2% agarose diluted in PBS were infused into the lung via the trachea to expand alveoli. After dissection with the associated trachea, the lungs were kept in the inflated form in a histology cassette for further immersion fixation in 4% w/v PFA for 1 h at +4°C, and were then washed with PBS and incubated with 25% w/v sucrose before frozen embedding in the OCT Compound (Fisher HealthCare 4585). Twenty-μm frozen sections were cut, air-dried for 1 h,

permeabilized and blocked using Donkey Immunomix (PBS containing 5% v/v normal donkey serum, 0.2% w/v bovine serum albumin, 0.3% Triton-X and 0.05% w/v sodium azide) for 1 h, stained overnight at +4°C with primary antibodies, washed and then stained with secondary antibodies for 1-1.5 h at RT. Sections were then mounted with VECTASHILD Mounting Medium (Vector Laboratories, #H-1200). Samples were imaged using the Leica SP8 confocal microscope (Leica). For confocal images, 3D projections and orthogonal views were digitally reconstructed from Z stacks using ImageJ. Brightness and contrast of the images were adjusted uniformly to entire images using Adobe Photoshop where appropriate. Quantification of the percentage of CD44+ cells out of CD31+ ECs was performed on confocal images. A cell was identified as double positive only when they colocalized to the same cell from all xy, xz and yz views. A total of approximately 50 CD31+ cells per mouse were analyzed.

QUANTIFICATION AND STATISTICAL ANALYSIS

The majority of experiments were repeated two or more times as indicated in the figure legends. A few experiments were performed once, with $N \geq 3$ mice per group. Student's t test (2 groups) or one-way ANOVA (> 2 groups) were used to compare means. Two-way ANOVA was used when data from multiple experiments were pooled. When variances are unequal among different groups as determined by F test, logarithmic transformation to base 10 is used to compute the statistics. Data are presented as mean ± standard error of mean (SEM). Holm-Sidak test was used as a post hoc analysis when more than two groups were compared. Statistical analyses were carried out with Graphpad Prism (version 7), and the significance is indicated in the figures as follows: $p < 0.05$ (*), $p < 0.01$ (**), $p < 0.001$ (***), $p < 0.0001$ (****), and not significant (N.S.). For RNA-seq analysis, multiple hypothesis testing was adjusted using the Benjamini and Hochberg false-discovery-rate method.

Sample sizes for quantifications are as follows. Figures 1D and 1E: N = 4 mice for normal lungs and 8 mice pooled into 4 samples for metastases. Figure 1F: N = 4 samples pooled from 4 independent experiments, each pooled from 5-7 mice. N = 8 mice for WT in total. Figures 2B and 2C: N = 4 mice for normal lungs and 8 mice pooled into 4 samples for lung metastases. Figure 2H: N = 2-4 mice per group. Figures 3A and 3B, N = 6 mice for normal, 12 mice pooled into 5 samples for metastases, and 2 independent experiments are pooled. Figures 4C and 4D: N = 4 mice for normal lungs and 8 mice pooled into 4 samples for metastases. Figure 3E: N = 4 samples from 4 independent experiments, each pooled from 5-7 mice. Figure 3H: N = 7 mice pooled from 2 independent experiments. Figure 4C: N = 5-11 samples pooled from 10-22 mice from 3 independent experiments in total. Figure 4D: N = 2-6 pooled from 8-21 mice from 3 independent experiments in total. Figure 4E: N = 4-5 mice in total from two independent experiments. Figure 4F: N = 4-5 mice. All bar graphs represent means ± SEM. Lines in scatterplots indicate means.

DATA AND CODE AVAILABILITY

The accession number for RNA sequencing data deposited in NCBI Gene Expression Omnibus is GEO: GSE123520.